

# Visualization of Covariance Structures for Multivariate Spatio-Temporal Random Fields

Huang Huang\*      Ying Sun      Marc G. Genton  
Statistics Program  
King Abdullah University of Science and Technology

August 11, 2020

## Abstract

The prevalence of multivariate space-time data collected from monitoring networks and satellites or generated from numerical models has brought much attention to multivariate spatio-temporal statistical models, where the covariance function plays a key role in modeling, inference, and prediction. For multivariate space-time data, understanding the spatio-temporal variability, within and across variables, is essential in employing a realistic covariance model. Meanwhile, the complexity of generic covariances often makes model fitting very challenging, and simplified covariance structures, including symmetry and separability, can reduce the model complexity and facilitate the inference procedure. However, a careful examination of these properties is needed in real applications. In the work presented here, we formally define these properties for multivariate spatio-temporal random fields and use functional data analysis techniques to visualize them, hence providing intuitive interpretations. We then propose a rigorous rank-based testing procedure to conclude whether the simplified properties of covariance are suitable for the underlying multivariate space-time data. The good performance of our method is illustrated through synthetic data, for which we know the true structure. We also investigate the covariance of bivariate wind speed, a key variable in renewable energy, over a coastal and an inland area in Saudi Arabia.

*Keywords:* Bivariate Wind Vector, Functional Boxplot, Multivariate Spatio-Temporal Data, Rank-Based Test, Separability, Symmetry

---

\*huang.huang@kaust.edu.sa

# 1 Introduction

Multivariate spatio-temporal modeling has become a very active research area in many scientific fields, including climate, hydrology, and ecology, due to its capacity to capture the space-time characteristics of data and provide accurate statistical inference. For example, Paciorek and McLachlan (2009) used multivariate spatio-temporal models to uncover forest composition in history based on fossil pollen records; Zammit-Mangion et al. (2015) used a multivariate spatio-temporal Gaussian Markov random field to assess Antarctica’s mass balance and contribution to the rise of sea-level; Mastrantonio et al. (2019) used a multivariate spatio-temporal model in a Bayesian hierarchical framework to investigate the extreme temperatures and precipitation jointly. Gaussian random fields are widely used in geostatistics, directly representing the variables used in the study or serving as a building block in more complex statistical models, where the covariance structure plays a key role in quantifying dependence and providing prediction. Gneiting et al. (2010) developed valid Matérn covariance functions for multivariate spatial random fields. Apanasovich and Genton (2010) proposed new approaches to build valid multivariate spatio-temporal covariance models via latent dimensions. Genton and Kleiber (2015) reviewed approaches to build cross-covariance functions for multivariate random fields.

For real applications, the choice of the covariance model is case-specific. Understanding the spatio-temporal variability within and across variables is essential in choosing a realistic covariance model. In addition, with the development of remote sensing and *in situ* measurement techniques, and with powerful computing facilities that enable better physical model simulations, large data sets of unprecedented size are collected. It is often challenging and slow to perform the model inference because space-time covariance models typically involve many parameters that need to be estimated from data. Specific constraints on the proposed covariance structure can reduce the model complexity and accelerate the inference procedure. These considerations motivate researchers to study simplified covariance structures and propose tools to visualize and assess them. Cressie and Huang (1999) proposed several approaches to build univariate nonseparable spatio-temporal covariances with separable covariances as special cases. Gneiting et al. (2007) investigated both the univariate

separability and symmetry covariance structures. Graphical evidence for these univariate properties includes the contour plots in Cressie and Huang (1999) and the functional box-plot (Sun and Genton, 2011) of proposed test functions in Huang and Sun (2019). Formal testing approaches have also been developed for the assessment of these properties. Examples include the test based on spectral representations (Fuentes, 2006) and the likelihood ratio test (Mitchell et al., 2006) for the univariate separability property, the separability and symmetry tests from constructed contrasts of covariances (Li et al., 2007), and the rank-based testing procedure using functional data analysis techniques (Huang and Sun, 2019); see Chen et al. (2021) for a comprehensive review of univariate spatio-temporal covariance structures and models. When data are multivariate space-time, there are more types of covariance structures, and the assessment is more complicated. Wackernagel (2013) used graphical evidence to indicate multivariate separability and symmetry, and Li et al. (2008) extended their previous testing procedure of the univariate covariance to the multivariate case, using contrasts of covariances at chosen lags.

To the best of our knowledge, the description of the different types of multivariate spatio-temporal separability and symmetry properties is scattered in the literature and incomplete, and there has not been any work formally defining all the different types of multivariate spatio-temporal covariances. In this paper, we introduce possible types of separability and symmetry properties for the multivariate spatio-temporal covariance and give formal definitions. We then develop test functions associated with each of the properties and use functional data analysis techniques to visualize them. Our proposed visualization tool is a very fast approach to view these properties; there has not been such a tool developed yet in the multivariate setting. We also propose a rank-based testing procedure that can examine these properties quantitatively. For simplicity, we focus on a weakly stationary multivariate spatio-temporal random field  $\mathbf{Z}(\mathbf{s}, t) \in \mathbb{R}^p$  for location  $\mathbf{s} \in \mathbb{R}^d$  and time  $t \in \{1, \dots, l\}$ , where the matrix-valued covariance function  $\mathbf{C}(\mathbf{h}, u) = \text{cov}\{\mathbf{Z}(\mathbf{s}_1, t_1), \mathbf{Z}(\mathbf{s}_2, t_2)\}$  depends only on the space lag  $\mathbf{h} = \mathbf{s}_1 - \mathbf{s}_2$  and time lag  $u = t_1 - t_2$ .

Our paper is organized as follows: Section 2 defines multivariate spatio-temporal covariance properties to be studied and our proposed tools for property visualization and as-

assessment; Section 3 describes our new methodology to visualize our proposed test functions and formally test covariance properties; Section 4 uses synthetic data sets to demonstrate the performance of the proposed testing procedure; Section 5 provides an example where we apply our proposed tools to analyze bivariate hourly wind speed over a coastal and an inland area in Saudi Arabia; Section 6 summarizes our methods and presents research directions for future improvement.

## 2 Multivariate Spatio-Temporal Covariance Properties

For a  $p$ -variate weakly stationary spatio-temporal random field  $\mathbf{Z}(\mathbf{s}, t) = \{Z_1(\mathbf{s}, t), \dots, Z_p(\mathbf{s}, t)\}^\top$ , we denote the covariance between the  $i$ -th and  $j$ -th variable with space lag  $\mathbf{h}$  and time lag  $u$  as  $C_{ij}(\mathbf{h}, u) = \text{cov}\{Z_i(\mathbf{s} + \mathbf{h}, t + u), Z_j(\mathbf{s}, t)\}$ ,  $i, j = 1, \dots, p$ .

### 2.1 Symmetry structures

For a univariate spatio-temporal covariance, there is only one unique symmetry property. When extending it to the multivariate case, three different types of symmetry may occur. We call the covariance *symmetric in variables* if  $C_{ij}(\mathbf{h}, u) = C_{ji}(\mathbf{h}, u), \forall i, j = 1, \dots, p$ . This condition is equivalent to  $C_{ij}(\mathbf{h}, u) = C_{ij}(-\mathbf{h}, -u)$  due to the fact that  $C_{ij}(\mathbf{h}, u) = C_{ji}(-\mathbf{h}, -u)$  naturally holds. We call the covariance *symmetric in space* if  $C_{ij}(\mathbf{h}, u) = C_{ij}(-\mathbf{h}, u), \forall i, j = 1, \dots, p$  and similarly *symmetric in time* if  $C_{ij}(\mathbf{h}, u) = C_{ij}(\mathbf{h}, -u), \forall i, j = 1, \dots, p$ . We also call the covariance *fully symmetric* if all types of symmetry apply, i.e.,  $C_{ij}(\mathbf{h}, u) = C_{ji}(\mathbf{h}, u) = C_{ij}(-\mathbf{h}, u) = C_{ij}(\mathbf{h}, -u), \forall i, j = 1, \dots, p$ . The three types of symmetry (*symmetry in variables*, *symmetry in space*, and *symmetry in time*) are not independent, and Proposition 2.1 shows the constraints among them with the proof given in the Appendix.

**Proposition 2.1.** *Any two types of symmetry in variables, space, and time imply the third type of symmetry and then the covariance is fully symmetric.*

## 2.2 Separability structures

For univariate spatio-temporal random fields, separability assumes no interaction between space and time, and separability implies symmetry. Although the assumption of separability is often unrealistic, it provides an easy solution to construct valid space-time covariance functions by the product of purely spatial and purely temporal covariance functions. It also eases the computations because the associated covariance matrix is a Kronecker product of purely spatial and purely temporal covariance matrices of much smaller sizes (Genton, 2007). For multivariate spatio-temporal random fields, there are more types of separability, and we define them in Table 1, which also shows the connection of multivariate spatio-temporal separability properties with symmetry properties, if there is one. We introduce some abbreviated notations for ease of presentation: V|ST, *separability between variables and space-time*; S|VT, *separability between space and variables-time*; T|VS, *separability between time and variables-space*; V|S, *separability between variables and space*; V|T, *separability between variables and time*; S|T, *separability between space and time*;  $V^{\text{sym}}$ , *symmetry in variables*;  $S^{\text{sym}}$ , *symmetry in space*;  $T^{\text{sym}}$ , *symmetry in time*.

Table 1: Definition of different types of separability properties. For each type, the covariance function can be written as two components, one of which is a general function concerning only a part of variables, space, and time, denoted by  $\rho$ . For example,  $\rho_1(\mathbf{h}, u)$  is a function with respect to only space and time. There are some natural equalities for these functions  $\rho$ : all these functions equal 1 when  $\mathbf{h} = \mathbf{0}$  and  $u = 0$ ,  $\rho_4(\mathbf{0}, u) = 1$  for any  $u$ , and  $\rho_5(\mathbf{h}, 0) = 1$  for any  $\mathbf{h}$ .

Type	Definition	Implication
V ST	$C_{ij}(\mathbf{h}, u) = \rho_1(\mathbf{h}, u)C_{ij}(\mathbf{0}, 0)$	$V^{\text{sym}}$
S VT	$C_{ij}(\mathbf{h}, u) = \rho_2(\mathbf{h})C_{ij}(\mathbf{0}, u)$	$S^{\text{sym}}$
T VS	$C_{ij}(\mathbf{h}, u) = \rho_3(u)C_{ij}(\mathbf{h}, 0)$	$T^{\text{sym}}$
V S	$C_{ij}(\mathbf{h}, u) = \rho_4(\mathbf{h}, u)C_{ij}(\mathbf{0}, u)$	
V T	$C_{ij}(\mathbf{h}, u) = \rho_5(\mathbf{h}, u)C_{ij}(\mathbf{h}, 0)$	
S T	$C_{ij}(\mathbf{h}, u) = \rho_{6,ij}(\mathbf{h})C_{ij}(\mathbf{0}, u)$	

One can clearly see that these six types can be grouped into two categories. The first category is that one component is completely separated from the other two. Though this may rarely happen for real data, the benefit brought by this property is significant because it allows us to write the covariance matrix as a Kronecker product of two smaller matrices. The three cases in this category are V|ST, S|VT, and T|VS. For example, when the covariance is V|ST, it can be decomposed into two parts corresponding to the correlation among variables ( $C_{ij}(\mathbf{0}, 0)$ ) and the spatio-temporal correlation ( $\rho_1(\mathbf{h}, u)$ ). This is also known as the *intrinsic correlation model* in Wackernagel (2013). We know  $C_{ij}(\mathbf{h}, u) = \rho_1(\mathbf{h}, u)C_{ij}(\mathbf{0}, 0) = \rho_1(\mathbf{h}, u)C_{ji}(\mathbf{0}, 0) = C_{ji}(\mathbf{h}, u)$ , so the multivariate spatio-temporal covariance is also  $V^{\text{sym}}$ .

The second category is the one for which no component in the covariance can be completely separated, but the interaction between certain two out of the three components is voided, which has less restriction than the first category described above. The three cases in the second category are V|S, V|T, and S|T. For example, when the covariance is V|S, there is no variable-space interaction, and the covariance can be decomposed into two parts corresponding to the variable-temporal correlation ( $C_{ij}(\mathbf{0}, u)$ ) and spatio-temporal correlation ( $\rho_4(\mathbf{h}, u)$ ). For cases in the second category, no symmetry property holds.

We also call a multivariate spatio-temporal covariance *fully separable* (denoted by  $F^{\text{sep}}$ ) if it satisfies all the separability properties, which implies *full symmetry* (denoted by  $F^{\text{sym}}$ ). Like symmetry, there are some constraints among different types of separability summarized in Propositions 2.2 through 2.4, proofs of which are given in the Appendix.

**Proposition 2.2.** *If a covariance is V|ST, then it is naturally V|S and V|T. Similarly, S|VT implies V|S and S|T, and T|VS implies V|T and S|T.*

**Proposition 2.3.** *If a covariance is V|S and V|T, then the covariance is V|ST. Similarly, V|S and S|T imply S|VT, and V|T and S|T imply T|VS.*

**Proposition 2.4.** *If any two properties of V|ST, S|VT, or T|VS hold, then the remaining one also holds and the covariance is  $F^{\text{sep}}$ .*

### 3 Methodology

#### 3.1 Test functions

We introduce our proposed test functions for the different covariance properties and show how we can use functional data analysis to visualize and assess the underlying properties. The test functions are a collection of realizations of random functions with respect to the temporal lag  $u$  based on the sample estimators of temporal covariances of the multivariate random field at every pair of locations. We denote by  $\hat{C}_{ij}^{a,b}(\mathbf{h}, u)$  the sample estimator of  $C_{ij}(\mathbf{h}, u)$  using samples  $\mathbf{Z}(\mathbf{s}_a, t)$  and  $\mathbf{Z}(\mathbf{s}_b, t)$  for  $t \in \{1, \dots, l\}$  and  $\mathbf{s}_a - \mathbf{s}_b = \mathbf{h}$ :

$$\hat{C}_{ij}^{a,b}(\mathbf{s}_a - \mathbf{s}_b, u) := \frac{1}{l-u} \sum_{t=1}^{l-u} \left\{ \mathbf{Z}_i(\mathbf{s}_a, t+u) - \frac{\sum_{r=1}^{l-u} \mathbf{Z}_i(\mathbf{s}_a, r+u)}{l-u} \right\} \left\{ \mathbf{Z}_j(\mathbf{s}_b, t) - \frac{\sum_{r=1}^{l-u} \mathbf{Z}_j(\mathbf{s}_b, r)}{l-u} \right\}.$$

Then, the different test functions for examining the corresponding symmetry types are shown in Table 2. The index is selected such that trivial zero curves and redundant flipped functional realizations are removed.

Table 2: Definition of test functions for different types of symmetry.

Type	Test Functions
V <sup>sym</sup>	$g_{i,j,a,b}^v(u) := \hat{C}_{ij}^{a,b}(\mathbf{s}_a - \mathbf{s}_b, u) - \hat{C}_{ji}^{a,b}(\mathbf{s}_a - \mathbf{s}_b, u), u \geq 0, i < j$
S <sup>sym</sup>	$g_{i,j,a,b}^s(u) := \hat{C}_{ij}^{a,b}(\mathbf{s}_a - \mathbf{s}_b, u) - \hat{C}_{ij}^{b,a}(\mathbf{s}_b - \mathbf{s}_a, u), u \geq 0; i \leq j, a < b$ or $i > j, a > b$
T <sup>sym</sup>	$g_{i,j,a,b}^t(u) := \hat{C}_{ij}^{a,b}(\mathbf{s}_a - \mathbf{s}_b, u) - \hat{C}_{ij}^{a,b}(\mathbf{s}_a - \mathbf{s}_b, -u), u > 0; i < j$ or $i = j, a \neq b$

For constructing test functions for separability, in addition to estimating  $C_{ij}(\mathbf{h}, u)$ , we also need to estimate all the functions  $\rho_1(\mathbf{h}, u)$ ,  $\rho_2(\mathbf{h})$ ,  $\rho_3(u)$ ,  $\rho_4(\mathbf{h}, u)$ ,  $\rho_5(\mathbf{h}, u)$ , and  $\rho_{6,ij}(\mathbf{h})$  given the observations  $\mathbf{Z}(\mathbf{s}_a, t)$  and  $\mathbf{Z}(\mathbf{s}_b, t)$  for  $t \in \{1, \dots, l\}$ . There can be various ways to estimate them. For example,  $\hat{\rho}_1^{a,b}(\mathbf{s}_b - \mathbf{s}_a, u)$ , given samples  $\mathbf{Z}(\mathbf{s}_a, t)$  and  $\mathbf{Z}(\mathbf{s}_b, t)$ , can be  $\sum_{i,j=1}^p [2\hat{C}_{ij}^{a,b}(\mathbf{s}_a - \mathbf{s}_b, u) / \{\hat{C}_{ij}^{a,a}(\mathbf{0}, u) + \hat{C}_{ij}^{b,b}(\mathbf{0}, u)\}] / p$ , where we use the average of the estimator of  $\rho_1^{a,b}(\mathbf{s}_a - \mathbf{s}_b, u)$  from all possible combinations of components. However, we use a least square estimator by fitting to a regression line as follows in our analysis for the

purpose of more robust estimation,

$$\hat{\rho}_1^{a,b}(\mathbf{s}_a - \mathbf{s}_b, u) = \frac{2 \sum_{i,j=1}^p \hat{C}_{ij}^{a,b}(\mathbf{s}_b - \mathbf{s}_a, u) \{\hat{C}_{ij}^{a,a}(\mathbf{0}, 0) + \hat{C}_{ij}^{b,b}(\mathbf{0}, 0)\}}{\sum_{i,j=1}^p \{\hat{C}_{ij}^{a,a}(\mathbf{0}, 0) + \hat{C}_{ij}^{b,b}(\mathbf{0}, 0)\}^2}.$$

All the other required estimators are

$$\begin{aligned} \hat{\rho}_2^{a,b}(u) &= \frac{\sum_{i,j=1}^p \{\hat{C}_{ij}^{a,a}(\mathbf{0}, u) + \hat{C}_{ij}^{b,b}(\mathbf{0}, u)\} \{\hat{C}_{ij}^{a,a}(\mathbf{0}, 0) + \hat{C}_{ij}^{b,b}(\mathbf{0}, 0)\}}{\sum_{i,j=1}^p \{\hat{C}_{ij}^{a,a}(\mathbf{0}, 0) + \hat{C}_{ij}^{b,b}(\mathbf{0}, 0)\}^2}, \\ \hat{\rho}_3^{a,b}(\mathbf{s}_a - \mathbf{s}_b) &= \frac{2 \sum_{i,j=1}^p \hat{C}_{ij}^{a,b}(\mathbf{s}_a - \mathbf{s}_b, 0) \{\hat{C}_{ij}^{a,a}(\mathbf{0}, 0) + \hat{C}_{ij}^{b,b}(\mathbf{0}, 0)\}}{\sum_{i,j=1}^p \{\hat{C}_{ij}^{a,a}(\mathbf{0}, 0) + \hat{C}_{ij}^{b,b}(\mathbf{0}, 0)\}^2}, \\ \hat{\rho}_4^{a,b}(\mathbf{s}_a - \mathbf{s}_b, u) &= \frac{2 \sum_{i,j=1}^p \hat{C}_{ij}^{a,b}(\mathbf{s}_a - \mathbf{s}_b, u) \{\hat{C}_{ij}^{a,a}(\mathbf{0}, u) + \hat{C}_{ij}^{b,b}(\mathbf{0}, u)\}}{\sum_{i,j=1}^p \{\hat{C}_{ij}^{a,a}(\mathbf{0}, u) + \hat{C}_{ij}^{b,b}(\mathbf{0}, u)\}^2}, \\ \hat{\rho}_5^{a,b}(\mathbf{s}_a - \mathbf{s}_b, u) &= \frac{\sum_{i,j=1}^p \hat{C}_{ij}^{a,b}(\mathbf{s}_a - \mathbf{s}_b, u) \hat{C}_{ij}^{a,b}(\mathbf{s}_a - \mathbf{s}_b, 0)}{\sum_{i,j=1}^p \hat{C}_{ij}^{a,b}(\mathbf{s}_a - \mathbf{s}_b, 0)^2}, \\ \hat{\rho}_{6,ij}^{a,b}(\mathbf{s}_a - \mathbf{s}_b) &= 2 \hat{C}_{ij}^{a,b}(\mathbf{s}_a - \mathbf{s}_b, 0) / \{\hat{C}_{ij}^{a,a}(\mathbf{0}, 0) + \hat{C}_{ij}^{b,b}(\mathbf{0}, 0)\}. \end{aligned}$$

We then build test functions for different types of separability. Instead of looking at the difference between the original covariance and its decomposition directly, we focus on the difference between these differences from the same variable and the average of different variables, except S|T, to make it more obvious in visualizing non-separability. Table 3 summarizes our proposed test functions for separability.

## 3.2 Visualization of test functions

We see that, under the symmetry or separability assumption, the expectation of the associated test functions is zero. The deviation of test functions from zero suggests that the underlying assumption is violated. To visualize the proposed test functions, we make use of functional boxplots proposed by Sun and Genton (2011), with some modification and extension to focus on the deviation from zero.

Figure 1 shows examples of our visualization tools of test functions  $f^{s|vt}$ . Figure 1 (a) illustrates our modified functional boxplot for  $f^{s|vt}$  obtained from simulated data with a S|VT covariance. The obtained test functions are first ordered by the modified band depth (López-Pintado and Romo, 2009), then the 50% central region that consists of the 50% test functions with largest band depth values is shown as the area bordered by the



Table 3: Definition of test functions for different types of separability.

Type	Test Functions
V ST	$f_{i,a,b}^{v st}(u) := \tilde{f}_{i,j,a,b}^{v st}(u) - \frac{1}{p-1} \sum_{j \neq i} \tilde{f}_{i,j,a,b}^{v st}(u), u > 0,$ <p>where <math>\tilde{f}_{i,j,a,b}^{v st}(u) := \hat{C}_{ij}^{a,b}(\mathbf{s}_b - \mathbf{s}_a, u) - \frac{1}{2} \hat{\rho}_1^{a,b}(\mathbf{s}_b - \mathbf{s}_a, u) \{ \hat{C}_{ij}^{a,a}(\mathbf{0}, 0) + \hat{C}_{ij}^{b,b}(\mathbf{0}, 0) \}</math></p>
S VT	$f_{i,a,b}^{s vt}(u) := \tilde{f}_{i,j,a,b}^{s vt}(u) - \frac{1}{p-1} \sum_{j \neq i} \tilde{f}_{i,j,a,b}^{s vt}(u), u > 0, a \neq b,$ <p>where <math>\tilde{f}_{i,j,a,b}^{s vt}(u) := \hat{C}_{ij}^{a,b}(\mathbf{s}_a - \mathbf{s}_b, u) - \frac{1}{2} \hat{\rho}_2^{a,b}(\mathbf{s}_a - \mathbf{s}_b, u) \{ \hat{C}_{ij}^{a,a}(\mathbf{0}, u) + \hat{C}_{ij}^{b,b}(\mathbf{0}, u) \}</math></p>
T VS	$f_{i,a,b}^{t vs}(u) := \tilde{f}_{i,j,a,b}^{t vs}(u) - \frac{1}{p-1} \sum_{j \neq i} \tilde{f}_{i,j,a,b}^{t vs}(u), u > 0,$ <p>where <math>\tilde{f}_{i,j,a,b}^{t vs}(u) := \hat{C}_{ij}^{a,b}(\mathbf{s}_a - \mathbf{s}_b, u) - \hat{\rho}_3^{a,b}(u) \hat{C}_{ij}^{a,b}(\mathbf{s}_a - \mathbf{s}_b, 0)</math></p>
V S	$f_{i,a,b}^{v s}(u) := \tilde{f}_{i,j,a,b}^{v s}(u) - \frac{1}{p-1} \sum_{j \neq i} \tilde{f}_{i,j,a,b}^{v s}(u), u > 0, a \neq b$ <p>where <math>\tilde{f}_{i,j,a,b}^{v s}(u) := \hat{C}_{ij}^{a,b}(\mathbf{s}_a - \mathbf{s}_b, u) - \frac{1}{2} \hat{\rho}_4^{a,b}(\mathbf{s}_a - \mathbf{s}_b, u) \{ \hat{C}_{ij}^{a,a}(\mathbf{0}, u) + \hat{C}_{ij}^{b,b}(\mathbf{0}, u) \},</math></p>
V T	$f_{i,a,b}^{v t}(u) := \tilde{f}_{i,j,a,b}^{v t}(u) - \frac{1}{p-1} \sum_{j \neq i} \tilde{f}_{i,j,a,b}^{v t}(u), u > 0,$ <p>where <math>\tilde{f}_{i,j,a,b}^{v t}(u) := \hat{C}_{ij}^{a,b}(\mathbf{s}_a - \mathbf{s}_b, u) - \hat{\rho}_5^{a,b}(\mathbf{s}_a - \mathbf{s}_b, u) \hat{C}_{ij}^{a,b}(\mathbf{s}_a - \mathbf{s}_b, 0)</math></p>
S T	$f_{i,a,b}^{s t}(u) := \hat{C}_{ij}^{a,b}(\mathbf{s}_a - \mathbf{s}_b, u) - \frac{1}{2} \hat{\rho}_6^{a,b}(\mathbf{s}_a - \mathbf{s}_b, u) \{ \hat{C}_{ij}^{a,a}(\mathbf{0}, u) + \hat{C}_{ij}^{b,b}(\mathbf{0}, u) \}, u > 0, a \neq b$

blue box. The original functional boxplot of Sun and Genton (2011) fills the central region with solid magenta color. To better show the relative position of test functions to zero, we fill the central region above zero with solid magenta, but fill the central region below zero with dashed magenta lines. These two parts in the central region suggest that the underlying covariance is S|VT. The upper- and lower-blue curves are the whiskers, which are the envelop of test functions within the inflated central region by 1.5 times the height of the central region at each  $u$ . Figure 1 (b) and (c) are discussed in Section 3.3 after the testing procedure is introduced.

### 3.3 Testing covariance properties

After obtaining the test functions, we can perform hypothesis tests for covariance properties based on nonparametric functional data ranking. We use a similar testing procedure to that introduced by Huang and Sun (2019) for a univariate spatio-temporal covariance. The

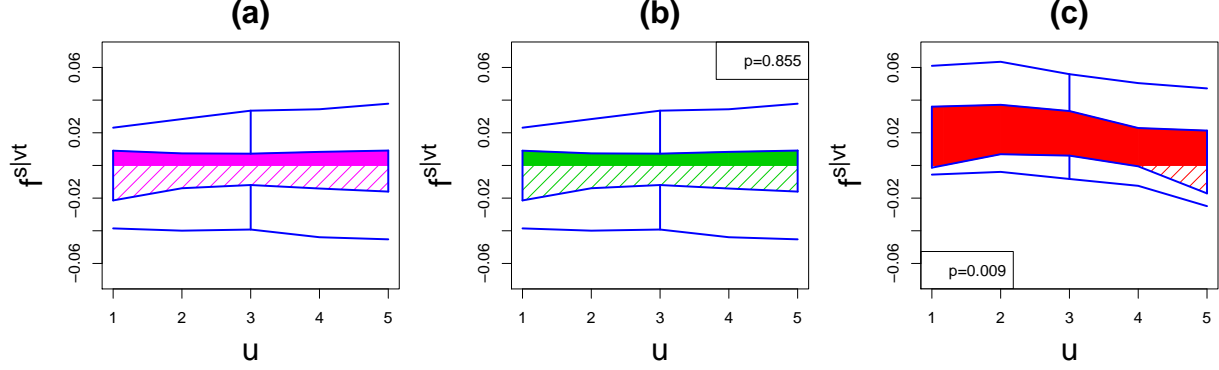


Figure 1: Examples of visualization of test functions  $f^{s|vt}$ . (a) and (b): the modified functional boxplots of  $f^{s|vt}$  from simulated data with S|VT covariance where the hypothesis test is not applied and applied, respectively. (c): the modified functional boxplot of  $f^{s|vt}$  from simulated data with covariance that is not S|VT where the hypothesis test is applied.

key idea is to test whether two functional data sets are from the same distribution (López-Pintado and Romo, 2009), which requires to generate reference data under the null covariance model described in Table 4. Figure 2 illustrates the entire testing procedure.

Table 4: Constructed covariance  $\hat{\mathbf{C}}^{H_0}(\mathbf{h}, u)$  for different types of property in  $H_0$ .

Type	$\hat{\mathbf{C}}^{H_0}(\mathbf{h}, u)$
V <sup>sym</sup>	$\hat{C}_{ij}^{H_0}(\mathbf{h}, u) := \{\hat{C}_{ij}(\mathbf{h}, u) + \hat{C}_{ji}(\mathbf{h}, u)\}/2$
S <sup>sym</sup>	$\hat{C}_{ij}^{H_0}(\mathbf{h}, u) := \{\hat{C}_{ij}(\mathbf{h}, u) + \hat{C}_{ij}(-\mathbf{h}, u)\}/2$
T <sup>sym</sup>	$\hat{C}_{ij}^{H_0}(\mathbf{h}, u) := \{\hat{C}_{ij}(\mathbf{h}, u) + \hat{C}_{ij}(\mathbf{h}, -u)\}/2$
V ST	$\hat{C}_{ij}^{H_0}(\mathbf{h}, u) := \hat{\rho}_1(\mathbf{h}, u)\hat{C}_{ij}(\mathbf{0}, 0)$
S VT	$\hat{C}_{ij}^{H_0}(\mathbf{h}, u) := \hat{\rho}_2(\mathbf{h})\hat{C}_{ij}(\mathbf{0}, u)$
T VS	$\hat{C}_{ij}^{H_0}(\mathbf{h}, u) := \hat{\rho}_3(u)\hat{C}_{ij}(\mathbf{h}, 0)$
V S	$\hat{C}_{ij}^{H_0}(\mathbf{h}, u) := \hat{\rho}_4(\mathbf{h}, u)\hat{C}_{ij}(\mathbf{0}, u)$
V T	$\hat{C}_{ij}^{H_0}(\mathbf{h}, u) := \hat{\rho}_5(\mathbf{h}, u)\hat{C}_{ij}(\mathbf{h}, 0)$
S T	$\hat{C}_{ij}^{H_0}(\mathbf{h}, u) := \hat{\rho}_{6,ij}(\mathbf{h})\hat{C}_{ij}(\mathbf{0}, u)$

For ease of presentation,  $g(u)$  denotes the test function for an arbitrary property. We denote by  $H_0$  the underlying null hypothesis and by  $H_a$  the alternative hypothesis. For

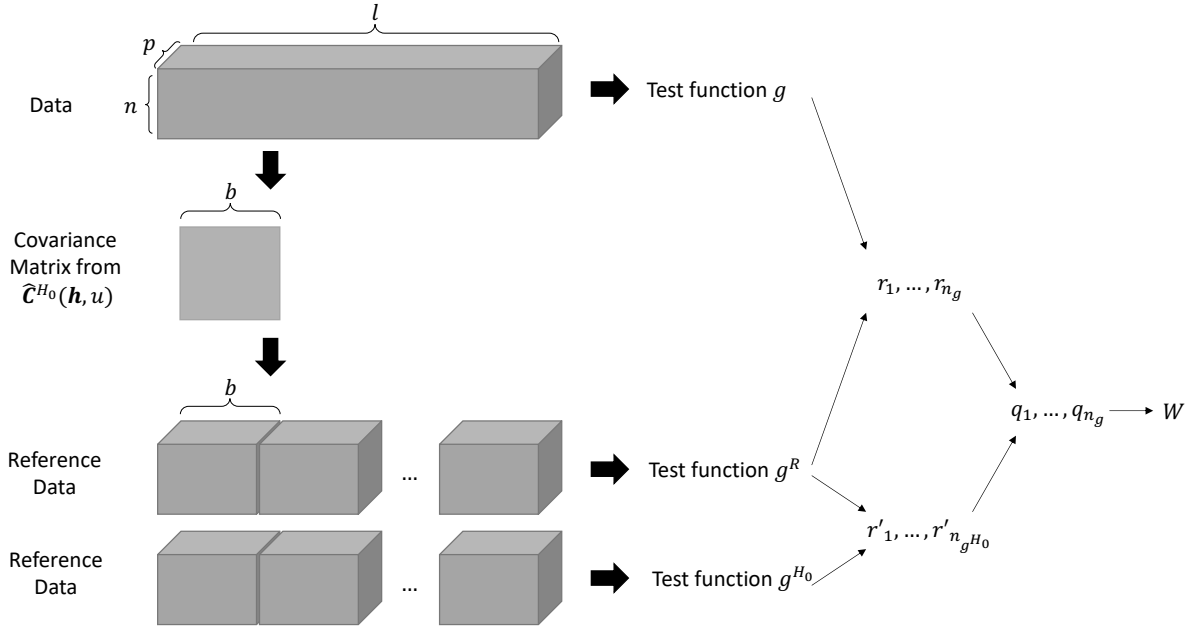


Figure 2: Flow chart of the proposed hypothesis testing procedure.

example, when we test  $V^{\text{sym}}$ ,  $g(u)$  is  $g_{i,j,a,b}^v(u)$ ,  $H_0$  is symmetry in variables, and  $H_a$  is asymmetry in variables. To perform the hypothesis test, the realizations of test functions  $g$  from the data are obtained. Then, the constructed covariance  $\hat{\mathbf{C}}^{H_0}(\mathbf{h}, u) = (C_{ij}^{H_0}(\mathbf{h}, u))_{i,j=1,\dots,p}$  under  $H_0$  described in Table 4 based on sample estimators  $\hat{C}_{ij}(\mathbf{h}, u)$ ,  $\hat{\rho}_1(\mathbf{h}, u)$ ,  $\hat{\rho}_2(\mathbf{h})$ ,  $\hat{\rho}_3(u)$ ,  $\hat{\rho}_4(\mathbf{h}, u)$ ,  $\hat{\rho}_5(\mathbf{h}, u)$ , or  $\hat{\rho}_{6,ij}(\mathbf{h})$  of the original data is used to generate two independent reference data sets. We calculate the test functions from these two reference data sets, denoted by  $g^{H_0}$  and  $g^R$ . The superscript “R” stands for reference. It is noteworthy that there is no difference in obtaining  $g^{H_0}$  and  $g^R$ , both of which are test functions obtained from simulated data samples with the same covariance under  $H_0$ . We simply use one of them as a reference and denote it by  $g^R$ . We know that, in principle,  $g^{H_0}$  and  $g^R$  are close to zero. Then, the rank-based test for the functional data is used. Suppose there are  $n_g$  and  $n_{gH_0}$  curves in  $g$  and  $g^{H_0}$ , respectively. For each curve in  $g$ , mix it with all curves in  $g^R$ , and calculate its rank using an increasing order of modified band depths (López-Pintado and Romo, 2009). Denote all these ranks by  $r_1, r_2, \dots, r_{n_g}$ . Do the same for  $g^{H_0}$ , and calculate the rank of each curve in  $g^{H_0}$  among  $g^R$ , denoted by  $r'_1, r'_2, \dots, r'_{n_{gH_0}}$ . Mix  $r_1, r_2, \dots, r_{n_g}$  with

$r'_1, r'_2, \dots, r'_{n_{gH_0}}$  and calculate the ranks of  $r_1, r_2, \dots, r_{n_g}$  in an increasing order, denoted by  $q_1, q_2, \dots, q_{n_g}$ . The final test statistic is

$$W = \frac{1}{n_g} \times \frac{\sum_{i=1}^{n_g} q_i}{n_g + n_{gH_0}}.$$

The limiting distribution of  $W$  under  $H_0$  is the sum of  $n_g$  samples from the integer sequence  $1, \dots, n_g + n_{gH_0}$ . Given the general small values of  $n_g$  and  $n_{gH_0}$  in practice, we use bootstrap to determine the distribution of  $W$  under the null hypothesis  $H_0$  and obtain the critical values for arbitrary significance levels.

We modify some parts in the previously proposed testing procedure for the univariate spatio-temporal covariance (Huang and Sun, 2019) and extend it to be suitable for multivariate cases to facilitate computations. The most challenging part of performing the test is to generate the reference data set. Since the original data are multivariate spatio-temporal, the dimension of the covariance matrix is very large if we generate the reference data set as a whole, causing memory and computational issues. A more feasible approach is to generate the reference data block by block with a block size  $b$  and assume that each block is only correlated with the previous block when  $b$  is big enough. However, we find some sensitivity issues associated with this approach in our study—a small error in the conditional distribution due to the noise in the sample estimators of the covariance could lead to blow-up in this sequential conditional generation. To resolve this issue, we use purely independent blocks when generating the reference data set. This may lead to inconsistency in the generated reference data set to some extent. However, the obtained  $g^{H_0}$  and  $g^R$  can still reflect the correct variability when  $b$  is not small, according to the results of our simulation study in Section 4. In general, when  $b$  is larger, this artifact is more alleviated. However, a larger  $b$  causes more computation burden and memory consumption. We use a parameter `max.mat.dim` to determine the size of the intermediate covariance matrix needed in the generation of reference data. There is a relationship between `max.mat.dim` and the allowed maximum  $b$ : `max.mat.dim`  $\geq p \times n \times \min(b, l)$  (recall that  $p$  is the number of variables,  $n$  is the number of locations, and  $l$  is the number of time points) for  $V^{\text{sym}}$ ,  $S^{\text{sym}}$ ,  $T^{\text{sym}}$ ,  $V|S$ ,  $V|T$ , and  $S|T$ ; `max.mat.dim`  $\geq \max(p, n \times \min(b, l))$  for  $V|ST$  because the needed covariance matrix can be written as a Kronecker product of two parts; `max.mat.dim`

$\geq \max(n, p \times \min(b, l))$  for S|VT; and  $\text{max.mat.dim} \geq \max(p \times n, \min(b, l))$  for T|VS. One can set `max.mat.dim` to the maximum value that is feasible for the computer in use. In our simulation study in Section 4, we use `max.mat.dim` = 3000, which is realistic for most laptops and desktops. We obtain results with good performance, and observe that in our simulation cases, larger values of `max.mat.dim` do not lead to much different results but take much more computational time.

Figure 1 (b) displays the same test functions as in Figure 1 (a) but contains the results from the testing procedure explained above. We replace magenta with green because we obtain a p-value of 0.855, which implies the underlying covariance is S|VT if we use the significance level of 5%. Figure 1 (c) visualizes the test functions  $f^{s|vt}$  obtained from other simulated data with a covariance other than S|VT. We see that the central region deviates from zero. The hypothesis testing gives a p-value of 0.009, which rejects the null hypothesis, S|VT. Therefore, we use red instead of magenta to indicate the rejection of the underlying property. As has been discussed, the testing procedure needs much more computational time than just visualization. Our visualization tool uses magenta, if no hypothesis test is performed, and red or green according to the test results, if we conduct the hypothesis test, in displaying the central regions of the test functions.

## 4 Simulation Study

### 4.1 Visualization and assessment for symmetry property

To analyze the symmetry properties of multivariate spatio-temporal covariances, we consider a bivariate spatio-temporal random field  $\mathbf{Z}(\mathbf{s}, t) = \{Z_1(\mathbf{s}, t), Z_2(\mathbf{s}, t)\}^\top$  for  $l$  time points and  $n = m^2$  locations in the unit square, i.e.,  $t \in \{1, 2, \dots, l\}$  and  $\mathbf{s} \in \{0, 1/(m-1), \dots, (m-2)/(m-1), 1\} \times \{0, 1/(m-1), \dots, (m-2)/(m-1), 1\}$ . Model 4.1 is used to generate data with different types of asymmetric covariance.

**Model 4.1.** *The second variable  $Z_2(\mathbf{s}, t)$  is a univariate first-order autoregressive spatio-*

temporal random field with a weakly stationary isotropic spatial noise. More specifically,

$$\{Z_2(\mathbf{s}_1, t), \dots, Z_2(\mathbf{s}_n, t)\}^\top = \begin{cases} 0.5\{Z_2(\mathbf{s}_1, t-1), \dots, Z_2(\mathbf{s}_n, t-1)\}^\top + \boldsymbol{\varepsilon}_t & , t > 1 \\ \boldsymbol{\varepsilon}_t & , t = 1 \end{cases}$$

where  $\boldsymbol{\varepsilon}_1 \sim N_n(\mathbf{0}, \boldsymbol{\Sigma})$  and  $\boldsymbol{\varepsilon}_t \sim N_n(\mathbf{0}, \frac{3}{4}\boldsymbol{\Sigma})$  for  $t > 1$ . Here,  $\boldsymbol{\Sigma}$  is a matrix of dimension  $n \times n$  with  $(i, j)^{th}$  value  $\Sigma_{ij} = \exp(-2\|\mathbf{s}_i - \mathbf{s}_j\|)$  for  $i, j \in \{1, \dots, n\}$ . The first variable  $Z_1(\mathbf{s}, t)$  is defined as  $Z_1(\mathbf{s}, t) := \frac{\sqrt{2}}{2}Z_2(\mathbf{s} + \Delta_{\mathbf{s}}(\frac{1}{m-1}, \frac{1}{m-1}), t + \Delta_t) + \frac{\sqrt{2}}{2}\epsilon(\mathbf{s}, t)$ , where  $\epsilon(\mathbf{s}, t) \sim N(0, 1)$ ,  $\Delta_t \geq 0$  is the time lag, and  $\Delta_{\mathbf{s}}$  controls the distance of the spatial lag along the  $45^\circ$  direction. To make  $Z_1(\mathbf{s}, t)$  well defined,  $Z_2(\mathbf{s}, t)$  is generated in a larger spatial grid and a longer time window as  $\mathbf{s} \in \{0, 1/(m-1), \dots, (m-1+\Delta_{\mathbf{s}})/(m-1)\} \times \{0, 1/(m-1), \dots, (m-1+\Delta_{\mathbf{s}})/(m-1)\}$  and  $t \in \{1, 2, \dots, l + \Delta_t\}$ . However,  $Z_2(\mathbf{s}, t)$  is eliminated when  $\mathbf{s} \notin [0, 1] \times [0, 1]$  or  $t > l$  after obtaining all the needed  $Z_1(\mathbf{s}, t)$ .

Li et al. (2008) used a similar idea to Model 4.1 while only introducing  $\Delta_t$  in generating synthetic data with a symmetric or asymmetric covariance. One can clearly see that in Model 4.1,  $\Delta_{\mathbf{s}} = \Delta_t = 0$  leads to a fully symmetric random field,  $\Delta_{\mathbf{s}} \neq 0$  leads to a random field that is not  $V^{\text{sym}}$  or  $S^{\text{sym}}$ , and  $\Delta_t \neq 0$  leads to a random field that is not  $V^{\text{sym}}$  or  $T^{\text{sym}}$ .

Figure 3 exhibits all the test functions  $g^v$ ,  $g^s$ , and  $g^t$  of one random data set generated from Model 4.1 with  $m = 4$  and  $l = 10000$ . Four examples are shown with different combinations of chosen values of  $\Delta_{\mathbf{s}}$  and  $\Delta_t$  (denoted by  $D_{0,0}^{\text{sym}}$  when  $\Delta_{\mathbf{s}} = \Delta_t = 0$  and  $D_{\Delta_{\mathbf{s}}, \Delta_t}^{\text{asym}}$  when  $\Delta_{\mathbf{s}} \neq 0$  or  $\Delta_t \neq 0$ ). From the visualization and the obtained p-values in the hypothesis testing, we observe the conclusions coinciding with the truth that when  $\Delta_{\mathbf{s}} \neq 0$  or  $\Delta_t \neq 0$  the covariance is always not  $V^{\text{sym}}$ , and not  $S^{\text{sym}}$  or  $T^{\text{sym}}$  according to the non-zero  $\Delta_{\mathbf{s}}$  or  $\Delta_t$ . When both  $\Delta_{\mathbf{s}}$  and  $\Delta_t$  are non-zero, the covariance does not satisfy any property of  $V^{\text{sym}}$ ,  $S^{\text{sym}}$  and  $T^{\text{sym}}$ .

To show how the hypothesis testing performs in assessing the multivariate spatio-temporal symmetry property, we generate the four types of data  $D_{0,0}^{\text{sym}}$ ,  $D_{0,2}^{\text{asym}}$ ,  $D_{2,0}^{\text{asym}}$ , and  $D_{2,2}^{\text{asym}}$  with 1000 replicates. We use a significance level of 5% in the hypothesis testing, where `max.mat.dim` is set as 3000 and 1000 bootstraps are used. The results for the percentage of rejection replicates for each data type are given in Table 5. All the bold values indicate the associated properties hold for the particular data set, meaning the size of the

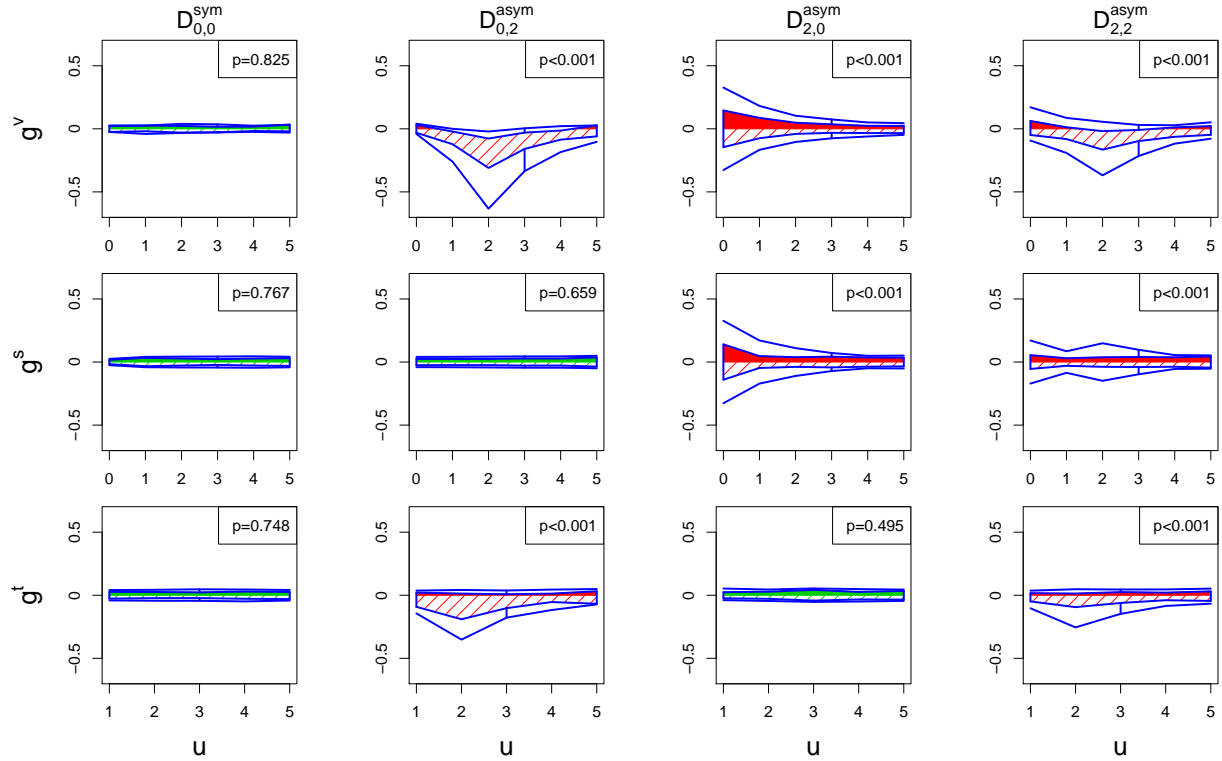


Figure 3: Visualization of symmetry test functions obtained from the simulated data  $D_{0,0}^{\text{sym}}$ ,  $D_{0,2}^{\text{asym}}$ ,  $D_{2,0}^{\text{asym}}$ , and  $D_{2,2}^{\text{asym}}$ .

Table 5: Percentage of rejections in 1000 replicates of data generated by Model 4.1 for each data type. All three types of symmetry properties are tested. Bold values are size, and others are power. Values in parentheses are estimated standard errors. The significance level is 5%, `max.mat.dim` is 3000, and 1000 bootstraps are used in the hypothesis test.

Type	$D_{0,0}^{\text{sym}}$	$D_{0,2}^{\text{asym}}$	$D_{2,0}^{\text{asym}}$	$D_{2,2}^{\text{asym}}$
$V^{\text{sym}}$	<b>5.1(0.7)</b>	100(0)	100(0)	100(0)
$S^{\text{sym}}$	<b>6.0(0.8)</b>	<b>6.5(0.8)</b>	100(0)	100(0)
$T^{\text{sym}}$	<b>5.6(0.7)</b>	100(0)	<b>5.3(0.7)</b>	100(0)

test. Since we use the significance level of 5%, the percentage of rejected cases should be ideally close to 5. We see the size tends to be slightly higher than the significance level, but still within two standard errors. All the other cases are reflecting the power, where the associated properties do not hold. We see the proposed hypothesis test has a very high

power, detecting asymmetric covariances in all the replicates.

## 4.2 Visualization and assessment for separability property

In this separability study, we also consider a zero-mean bivariate spatio-temporal random field  $\mathbf{Z}(\mathbf{s}, t) = \{Z_1(\mathbf{s}, t), Z_2(\mathbf{s}, t)\}^\top$  for  $t \in \{1, 2, \dots, l\}$  and  $\mathbf{s} \in \{0, 1/(m-1), \dots, (m-2)/(m-1), 1\} \times \{0, 1/(m-1), \dots, (m-2)/(m-1), 1\}$ . Following the way of building covariance models through latent dimensions by Apanasovich and Genton (2010) or using products of nonseparable functions by Gneiting (2002), we use a valid covariance function as used in Model 4.2.

**Model 4.2.** *The bivariate Gaussian process  $\mathbf{Z}(\mathbf{s}, t) = \{Z_1(\mathbf{s}, t), Z_2(\mathbf{s}, t)\}^\top$  has mean zero and the following covariance function:*

$$C_{ij}(\mathbf{h}, u) = \frac{1}{|i-j|+1} \exp\left(-\frac{|u/5|^2}{(|i-j|+1)^{\beta_1}}\right) \times \frac{1}{|u/5|+1} \exp\left(-\frac{\|\mathbf{h}\|^2}{(|u/5|+1)^{\beta_2}}\right).$$

We can easily observe that, when  $\beta_1 = \beta_2 = 0$ , the covariance is  $F^{\text{sep}}$ ; when  $\beta_1 = 0, \beta_2 \neq 0$ , the covariance is  $V|ST$ ,  $V|S$  and  $V|T$ ; when  $\beta_1 \neq 0, \beta_2 = 0$ , the covariance is  $S|VT$ ,  $V|S$  and  $S|T$ ; and when  $\beta_1 \neq 0, \beta_2 \neq 0$ , the covariance is  $V|S$ . Figure 4 exhibits all the test functions obtained from simulated data (denoted by  $D_{0,0}^{\text{sep}}$  when  $\beta_1 = \beta_2 = 0$  and denoted by  $D_{\beta_1, \beta_2}^{\text{nonsep}}$  when  $\beta_1 \neq 0$  or  $\beta_2 \neq 0$ ) with  $m = 4, l = 10000$  for different values of  $\beta_1$  and  $\beta_2$ . The visualization and obtained p-values reflect the correct covariance structure in theory. We also observe that the covariance built by Model 4.2 is always  $V|S$  because we do not add a variables-space interaction term in the formed covariance.

The size and power study of the hypothesis testing for the multivariate spatio-temporal separability property also uses the synthetic data from Model 4.2 with different values of  $\beta_1$  and  $\beta_2$ . To have more insights into the trend of power on non-zero  $\beta_1$  or  $\beta_2$  values, we use three distinct values 0, 0.5, 1 for both  $\beta_1$  and  $\beta_2$ . We still generate 1000 replicates for each data type and use a significance level of 5% in the test, where `max.mat.dim` is set as 3000 and 1000 bootstraps are used. The results for the number of rejection replicates for each data type are given in Table 6, where the bold values are the size and others are power. The obtained sizes are close to the true nominal level 5%, and the power generally



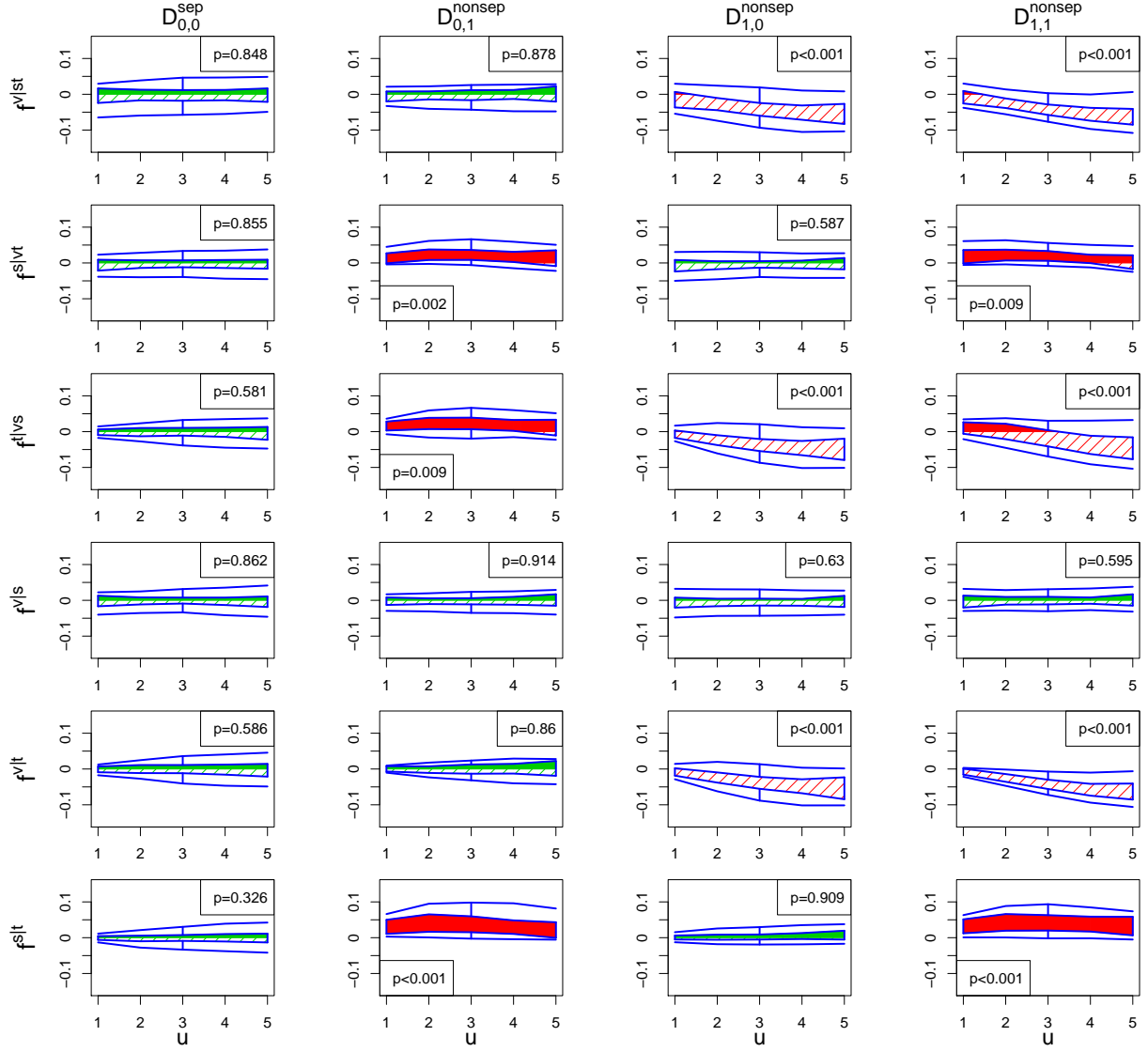


Figure 4: Visualization of separability test functions obtained from the simulated data  $D_{0,0}^{\text{sep}}$ ,  $D_{0,1}^{\text{nonsep}}$ ,  $D_{1,0}^{\text{nonsep}}$ , and  $D_{1,1}^{\text{nonsep}}$ .

increases as  $\beta_1$  or  $\beta_2$  increases when more interaction is introduced. For the most extreme case when  $\beta_1 = \beta_2 = 1$ , all the powers are above 95%.

Table 6: Percentage of rejection in 1000 replicates of data generated by Model 4.2 for each data type. All six types of separability properties are tested. Bold values are size, while others are power. Values in parentheses are estimated standard errors. The significance level is 5%, `max.mat.dim` is 3000, and 1000 bootstraps are used in the hypothesis testing.

Type	$\beta_1 = 0$			$\beta_1 = 0.5$			$\beta_1 = 1$		
	$\beta_2 = 0$	$\beta_2 = 0.5$	$\beta_2 = 1$	$\beta_2 = 0$	$\beta_2 = 0.5$	$\beta_2 = 1$	$\beta_2 = 0$	$\beta_2 = 0.5$	$\beta_2 = 1$
V   ST	<b>4.6(0.7)</b>	<b>4.3(0.6)</b>	<b>4.7(0.7)</b>	61.4(1.5)	67.0(1.5)	73.0(1.4)	99.6(0.2)	100(0)	99.9(0.1)
S   VT	<b>6.1(0.8)</b>	42.6(1.6)	99.0(0.3)	<b>6.4(0.8)</b>	33.4(1.5)	97.6(0.5)	<b>4.5(0.7)</b>	28.9(1.4)	95.9(0.6)
T   VS	<b>3.9(0.6)</b>	42.2(1.6)	99.7(0.2)	64.2(1.5)	73.7(1.4)	99.9(0.1)	99.9(0.1)	100(0)	100(0)
V   S	<b>6.1(0.8)</b>	<b>5.4(0.7)</b>	<b>5.1(0.7)</b>	<b>5.7(0.7)</b>	<b>5.7(0.7)</b>	<b>4.1(0.6)</b>	<b>5.2(0.7)</b>	<b>5.0(0.7)</b>	<b>6.5(0.8)</b>
V   T	<b>4.9(0.7)</b>	<b>4.2(0.6)</b>	<b>5.9(0.7)</b>	65.9(1.5)	74.9(1.4)	84.5(1.1)	99.8(0.1)	100(0)	100(0)
S   T	<b>6.0(0.8)</b>	100(0)	100(0)	<b>4.2(0.6)</b>	100(0)	100(0)	<b>4.6(0.7)</b>	100(0)	100(0)

## 5 Application to Bivariate Wind Data

In this section, we apply our visualization and assessment method to test the covariance structure in wind speed, which is a very important variable in many environmental studies. Wind farms and power grids are especially interested in obtaining sensible models of wind speed to better operate and manage the devices. For this purpose, we study the bivariate hourly wind speed in two areas in Saudi Arabia: one is an inland wind farm, Dumat Al Jandal, currently being built; the other one is a new mega-city, NEOM, in the northwestern coast, which is still under construction and expected to consume a large amount of renewable energy (wind and solar). The two areas are shown in Figure 5, where we choose  $5 \times 5 = 25$  locations in each area. We use the simulated high-resolution wind speed data in 2009, by the Weather Forecasting and Research (WRF) model from Yip (2018). The  $U$  and  $V$  components corresponding to two orthogonal directions of the wind speed are used as the bivariate variable. Figure 5 depicts the  $U$  and  $V$  components of the wind speed at 00:00, January 1st, 2009. After exploring the data set by Fourier transformation, we find strong periodic variability associated with 12-hour and 24-hour periods. Thus, we use a harmonic regression to remove the periodic mean and the intercept for each variable at each location as follows,

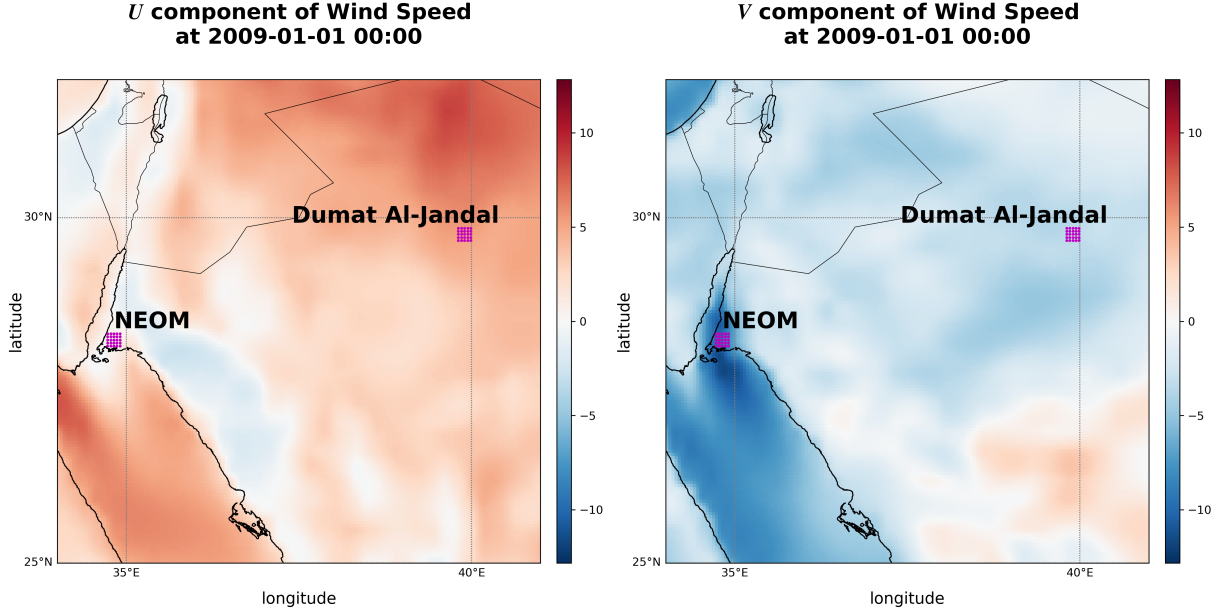


Figure 5: The bivariate wind speed at 00:00, January 1, 2009. A  $5 \times 5$  grid in each of the two areas (NEOM city and Dumat Al-Jandal wind farm) are selected, shown as the magenta points.

$$\begin{aligned}
 U(\mathbf{s}, t) &= \beta_{u,0}(\mathbf{s}) + \beta_{u,1}(\mathbf{s}) \cos(2\pi t/24) + \beta_{u,2}(\mathbf{s}) \sin(2\pi t/24) \\
 &\quad + \beta_{u,3}(\mathbf{s}) \cos(2\pi t/12) + \beta_{u,4}(\mathbf{s}) \sin(2\pi t/12) + \tilde{U}(\mathbf{s}, t), \\
 V(\mathbf{s}, t) &= \beta_{v,0}(\mathbf{s}) + \beta_{v,1}(\mathbf{s}) \cos(2\pi t/24) + \beta_{v,2}(\mathbf{s}) \sin(2\pi t/24) \\
 &\quad + \beta_{v,3}(\mathbf{s}) \cos(2\pi t/12) + \beta_{v,4}(\mathbf{s}) \sin(2\pi t/12) + \tilde{V}(\mathbf{s}, t).
 \end{aligned}$$

After the regression, the remaining process  $\mathbf{Z}(\mathbf{s}, t) := \{\tilde{U}(\mathbf{s}, t), \tilde{V}(\mathbf{s}, t)\}^\top$  becomes zero-mean, and we assess the covariance structure of  $\mathbf{Z}(\mathbf{s}, t)$ .

We analyze the bivariate hourly wind speed  $\mathbf{Z}(\mathbf{s}, t)$  for each month in 2009 and assume  $\mathbf{Z}(\mathbf{s}, t)$  is weakly stationary for each month. As revealed in previous studies, wind speed has often a strong interaction between space and time, and the prevailing wind direction generally makes the wind speed asymmetric. For this reason, we choose a less conservative significance level, 10%, to perform the hypothesis test.

For the symmetry test, we find that  $V^{\text{sym}}$  and  $S^{\text{sym}}$  are rejected in all cases. Figure 6 summarizes the p-values of testing  $T^{\text{sym}}$  for the two areas in each month. There are more

cases in NEOM when  $T^{\text{sym}}$  is not rejected, while only November in 2009 in Dumat Al-Jandal shows  $T^{\text{sym}}$ . We also observe that the covariance for all summer months (June, July, August) are not  $T^{\text{sym}}$ , inferring a more complex structure of wind in summer, due to potentially prevailing wind direction. Figure 7 gives two examples of the visualized test functions  $g^t$ .

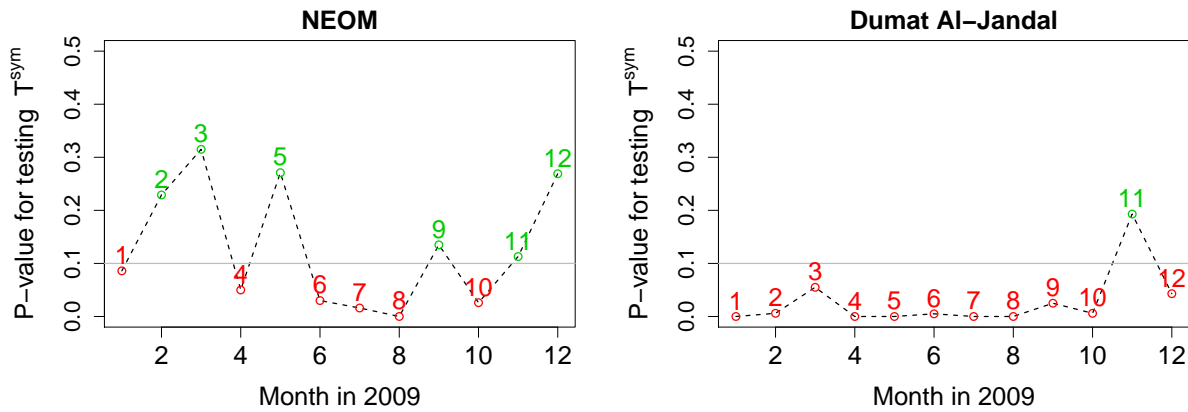


Figure 6: P-values of testing  $T^{\text{sym}}$  for the covariance in each month in NEOM and Dumat Al-Jandal. We show the month numbers in red if  $T^{\text{sym}}$  is rejected and in green otherwise, when using the significance level 10%.

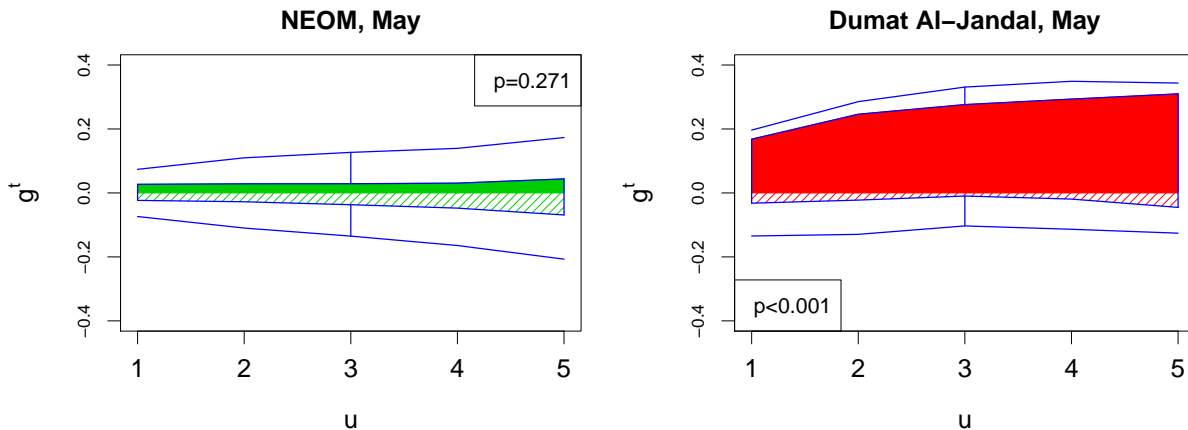


Figure 7: Visualization of test functions  $g^t$  in May, NEOM and Dumat Al-Jandal. The green plot shows  $g^t$  where  $T^{\text{sym}}$  is not rejected, and the red plot shows  $g^t$  where  $T^{\text{sym}}$  is rejected, when using the significance level 10%.

All the rejected symmetry assumptions lead to the rejection of the corresponding sepa-

rability assumptions of  $V|ST$ ,  $S|VT$ , and  $T|VS$ . We examined the rest and found that only  $V|T$  is not rejected in NEOM, and that  $V|T$  and  $S|T$  are not rejected in Dumat Al-Jandal for some months, where the p-values are given in Figure 8. For separability, we found an opposite behavior, namely that the covariance in Dumat Al-Jandal has more cases to be separable in particular forms than in NEOM. However, no separability properties in the first category ( $V|ST$ ,  $S|VT$ , and  $T|VS$ ) are observed, in any month, in any area, which implies it is generally inappropriate to use a reduced model that is a Kronecker product of its components in analyzing wind speed. Figure 9 gives examples of the visualized test functions  $f^{v|t}$  or  $f^{s|t}$ . It is noteworthy that the only two  $S|T$  cases, January and February in Dumat Al-Jandal, do not show  $V|T$ ; this is not surprising, because by Proposition 2.3, if both  $V|T$  and  $S|T$  hold, then the underlying covariance is  $S|VT$  and subsequently  $S^{\text{sym}}$ , but  $S^{\text{sym}}$  is rejected for these two cases.

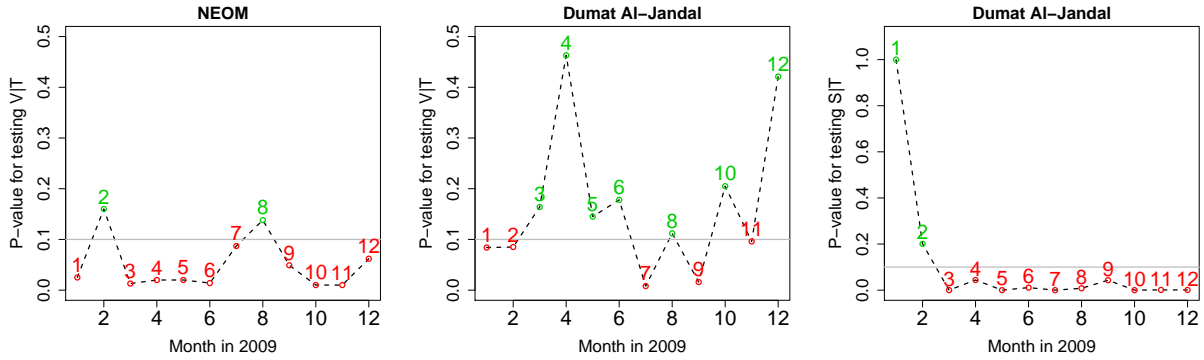


Figure 8: P-values of testing  $V|T$  or  $S|T$  for the covariance in each month in NEOM and Dumat Al-Jandal. We show the month numbers in red if the corresponding property  $V|T$  or  $S|T$  is rejected and in green otherwise, when using the significance level 10%.

## 6 Discussion

In this work, we elaborated on different types of symmetry and separability properties of multivariate spatio-temporal covariances. We developed test functions associated with each property to visualize and assess them. We used the functional boxplot with some modification to show test functions and get insights into the underlying covariance structures.

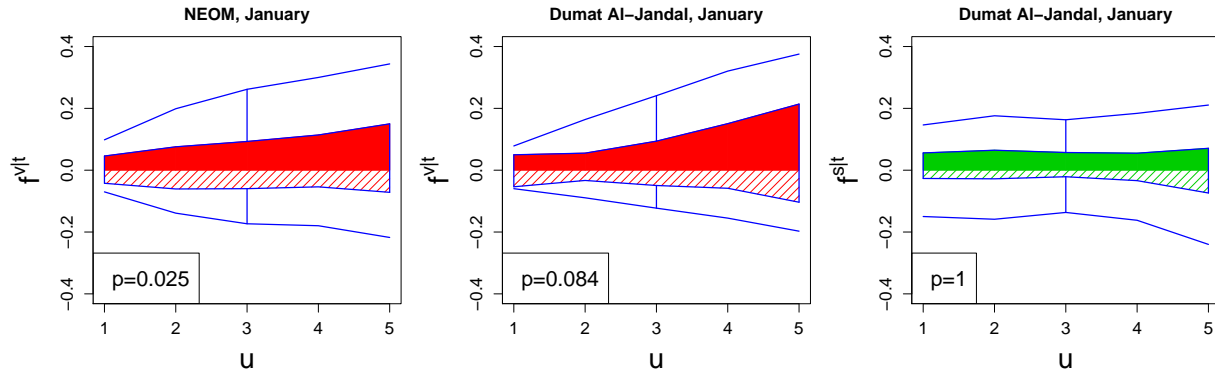


Figure 9: Visualization of test functions  $f^{v|t}$  or  $f^{s|t}$  in January, NEOM and Dumat Al-Jandal. The red plot shows  $f^{v|t}$  where  $V|T$  is rejected, and the green plot shows  $f^{s|t}$  where  $S|T$  is not rejected, when using the significance level 10%.

We proposed a rank-based hypothesis testing procedure to examine these properties in a more formal way, with a demonstrated good size and high power in the simulation study. We applied these tools to study the covariance of the bivariate wind speed in two areas of Saudi Arabia.

Obtaining and visualizing the test functions are always very fast. When a big deviation of test functions from zero is observed, one may directly proceed with covariance models that do not assume the corresponding simplified property. Otherwise, it may not be very clear if the underlying covariance property holds or not. The hypothesis testing is then needed to provide a better indication by p-values. However, the hypothesis testing is generally slower and needs more computational time.

It is noteworthy that we only showed examples of  $p = 2$  in the simulation and application studies because, for a larger  $p$ , one can always apply the visualization and assessment to every combination of two out of  $p$  variables and draw conclusions.

Our proposed testing procedure also has limitations. As we show in Section 2, there are some constraints on the covariance properties. What we proposed is an independent single testing scheme. In practice, there may be contradictory testing results from different independent tests. Developing a multi-testing framework may potentially resolve this problem. However, rigorous design and careful power studies are needed. This would be a direction for future research.

The R code (R Core Team, 2019) for our proposed visualization and test methods is provided in the supplementary materials (code.zip). In addition, an interactive R ShinyApp is also provided in the supplementary materials (shiny.zip) and available at <https://hhuang.shinyapps.io/mstCovariance>, where one can easily make different settings in the simulation examples described in Section 4 and see how the multivariate space-time covariance properties are changed.

## Acknowledgments

This publication is based on research supported by the King Abdullah University of Science and Technology (KAUST) Office of Sponsored Research (OSR) under Award No: OSR-2018-CRG7-3742 and in part by the Center of Excellence for NEOM Research at KAUST.

## Appendix

**Proof of Proposition 2.1:** We assume the covariance is *symmetric in space* and *symmetric in time*. Then, for any space lag  $\mathbf{h}$  and time lag  $u$ , we have  $C_{ij}(\mathbf{h}, u) = C_{ij}(-\mathbf{h}, u)$  by *symmetry in space* and  $C_{ij}(-\mathbf{h}, u) = C_{ij}(-\mathbf{h}, -u)$  by *symmetry in time*, for any  $i, j = 1, \dots, p$ . Therefore,  $C_{ij}(\mathbf{h}, u) = C_{ij}(-\mathbf{h}, -u), \forall i, j \in 1, \dots, p$ , which makes the covariance *symmetric in variables*. The proof is similar for other situations.  $\square$

**Proof of Proposition 2.2:** We assume the covariance is V|ST. Then, we know  $C_{ij}(\mathbf{h}, u) = \rho_1(\mathbf{h}, u)C_{ij}(\mathbf{0}, 0)$ . Plugging in  $\mathbf{h} = \mathbf{0}$ , we get  $C_{ij}(\mathbf{0}, u) = \rho_1(\mathbf{0}, u)C_{ij}(\mathbf{0}, 0)$ . Thus, we have  $C_{ij}(\mathbf{h}, u) = \rho_1(\mathbf{h}, u)C_{ij}(\mathbf{0}, u)/\rho_1(\mathbf{0}, u)$ . Let  $\rho_4(\mathbf{h}, u) := \rho_1(\mathbf{h}, u)/\rho_1(\mathbf{0}, u)$ , so we know  $\rho_4(\mathbf{0}, u) = 1, \forall u$  and  $C_{ij}(\mathbf{h}, u) = \rho_4(\mathbf{h}, u)C_{ij}(\mathbf{0}, u)$ , which is V|S. Similarly, plug in  $u = 0$  for the equation  $C_{ij}(\mathbf{h}, u) = \rho_1(\mathbf{h}, u)C_{ij}(\mathbf{0}, 0)$  and we get  $C_{ij}(\mathbf{h}, 0) = \rho_1(\mathbf{h}, 0)C_{ij}(\mathbf{0}, 0)$ . Thus,  $C_{ij}(\mathbf{h}, u) = \rho_1(\mathbf{h}, u)C_{ij}(\mathbf{h}, 0)/\rho_1(\mathbf{h}, 0)$ . Let  $\rho_5(\mathbf{h}, u) := \rho_1(\mathbf{h}, u)/\rho_1(\mathbf{h}, 0)$ . Then, we have  $\rho_5(\mathbf{h}, u) = 1, \forall \mathbf{h}$  and  $C_{ij}(\mathbf{h}, u) = \rho_5(\mathbf{h}, u)C_{ij}(\mathbf{0}, u)$ , which is V|T. The proof is similar for other situations.  $\square$

**Proof of Proposition 2.3:** We assume the covariance is V|S and V|T. Then,  $C_{ij}(\mathbf{h}, u) =$

$\rho_4(\mathbf{h}, u)C_{ij}(\mathbf{0}, u)$  and  $C_{ij}(\mathbf{h}, u) = \rho_5(\mathbf{h}, u)C_{ij}(\mathbf{h}, 0)$ , so we get the equation  $\rho_4(\mathbf{h}, u)C_{ij}(\mathbf{0}, u) = \rho_5(\mathbf{h}, u)C_{ij}(\mathbf{h}, 0)$ . Plugging in  $\mathbf{h} = \mathbf{0}$ , we have  $C_{ij}(\mathbf{0}, u) = \rho_5(\mathbf{0}, u)C_{ij}(\mathbf{h}, 0)/\rho_4(\mathbf{0}, u)$ . As  $\rho_4(\mathbf{0}, u) = 1$ , we know  $C_{ij}(\mathbf{0}, u) = \rho_5(\mathbf{0}, u)C_{ij}(\mathbf{h}, 0)$ . Therefore, we obtain  $C_{ij}(\mathbf{h}, u) = \rho_4(\mathbf{h}, u)\rho_5(\mathbf{0}, u)C_{ij}(\mathbf{0}, 0)$ . Let  $\rho_1(\mathbf{h}, u) := \rho_4(\mathbf{h}, u)\rho_5(\mathbf{0}, u)$ , and we have  $\rho_1(\mathbf{0}, 0) = \rho_4(\mathbf{0}, 0)\rho_5(\mathbf{0}, 0) = 1$ . Eventually, we get  $C_{ij}(\mathbf{h}, u) = \rho_1(\mathbf{h}, u)C_{ij}(\mathbf{0}, 0)$ , which is V|ST. The proof is similar for other situations.  $\square$

**Proof of Proposition 2.4:** We assume the covariance is V|ST and S|VT. By Proposition 2.2, we know the covariance is also V|T (as it is V|ST) and S|T (as it is S|VT). Then, by Proposition 2.3, the covariance is also T|VS. Moreover, V|S also holds from the fact that the covariance is V|ST. Therefore, all the separability properties hold, and the covariance is  $F^{\text{sep}}$ .  $\square$

## References

- Apanasovich, T. V. and Genton, M. G. (2010). Cross-covariance functions for multivariate random fields based on latent dimensions. *Biometrika*, 97(1):15–30.
- Chen, W., Genton, M. G., and Sun, Y. (2021). Space-time covariance structures and models. *Annual Review of Statistics and Its Application*, 8:to appear.
- Cressie, N. and Huang, H.-C. (1999). Classes of nonseparable, spatio-temporal stationary covariance functions. *Journal of the American Statistical Association*, 94(448):1330–1339.
- Fuentes, M. (2006). Testing for separability of spatial–temporal covariance functions. *Journal of Statistical Planning and Inference*, 136(2):447–466.
- Genton, M. G. (2007). Separable approximations of space-time covariance matrices. *Environmetrics*, 18(7):681–695.
- Genton, M. G. and Kleiber, W. (2015). Cross-covariance functions for multivariate geostatistics. *Statistical Science*, 30:147–163.



- Gneiting, T. (2002). Nonseparable, stationary covariance functions for space–time data. *Journal of the American Statistical Association*, 97(458):590–600.
- Gneiting, T., Genton, M. G., and Guttorp, P. (2007). Geostatistical space-time models, stationarity, separability, and full symmetry. In Finkenstädt, B., Held, L., and Isham, V., editors, *Statistical Methods for Spatio-temporal Systems*, pages 151–175. Chapman & Hall/CRC, Boca Raton.
- Gneiting, T., Kleiber, W., and Schlather, M. (2010). Matérn cross-covariance functions for multivariate random fields. *Journal of the American Statistical Association*, 105(491):1167–1177.
- Huang, H. and Sun, Y. (2019). Visualization and assessment of spatio-temporal covariance properties. *Spatial Statistics*, 34:100272.
- Li, B., Genton, M. G., and Sherman, M. (2007). A nonparametric assessment of properties of space–time covariance functions. *Journal of the American Statistical Association*, 102(478):736–744.
- Li, B., Genton, M. G., and Sherman, M. (2008). Testing the covariance structure of multivariate random fields. *Biometrika*, 95(4):813–829.
- López-Pintado, S. and Romo, J. (2009). On the concept of depth for functional data. *Journal of the American Statistical Association*, 104(486):718–734.
- Mastrantonio, G., Lasinio, G. J., Pollice, A., Capotorti, G., Teodonio, L., Genova, G., and Blasi, C. (2019). A hierarchical multivariate spatio-temporal model for clustered climate data with annual cycles. *Annals of Applied Statistics*, 13(2):797–823.
- Mitchell, M. W., Genton, M. G., and Gumpertz, M. L. (2006). A likelihood ratio test for separability of covariances. *Journal of Multivariate Analysis*, 97(5):1025–1043.
- Paciorek, C. J. and McLachlan, J. S. (2009). Mapping ancient forests: Bayesian inference for spatio-temporal trends in forest composition using the fossil pollen proxy record. *Journal of the American Statistical Association*, 104(486):608–622.

- R Core Team (2019). *R: A Language and Environment for Statistical Computing*. R Foundation for Statistical Computing, Vienna, Austria.
- Sun, Y. and Genton, M. G. (2011). Functional boxplots. *Journal of Computational and Graphical Statistics*, 20(2):316–334.
- Wackernagel, H. (2013). *Multivariate Geostatistics: An Introduction with Applications*. Springer Science & Business Media.
- Yip, C. M. A. (2018). *Statistical Characteristics and Mapping of Near-surface and Elevated Wind Resources in the Middle East*. PhD thesis, King Abdullah University of Science and Technology.
- Zammit-Mangion, A., Rougier, J., Schön, N., Lindgren, F., and Bamber, J. (2015). Multivariate spatio-temporal modelling for assessing Antarctica’s present-day contribution to sea-level rise. *Environmetrics*, 26(3):159–177.